J|A|C|S
ARTICLES
Published on Web 03/31/2007

Solid-State NMR Study of Amyloid Nanocrystals and Fibrils Formed by the Peptide GNNQQNY from Yeast Prion Protein Sup35p

Patrick C. A. van der Wel, Józef R. Lewandowski, and Robert G. Griffin*

Contribution from the Francis Bitter Magnet Laboratory and Department of Chemistry, Massachusetts Institute of Technology, Cambridge, Massachusetts 02139

Received December 1, 2006; E-mail: rgg@mit.edu

Abstract: Sup35p is a prion protein found in yeast that contains a prion-forming domain characterized by a repetitive sequence rich in Gln, Asn, Tyr, and Gly amino acid residues. The peptide $GNNQQNY_{7-13}$ is one of the shortest segments of this domain found to form amyloid fibrils, in a fashion similar to the protein itself. Upon dissolution in water, GNNQQNY displays a concentration-dependent polymorphism, forming monoclinic and orthorhombic crystals at low concentrations and amyloid fibrils at higher concentrations. We prepared nanocrystals of both space groups as well as fibril samples that reproducibly contain three (coexisting) structural forms and examined the specimens with magic angle spinning (MAS) solid-state nuclear magnetic resonance. ^{13}C and ^{15}N MAS spectra of both nanocrystals and fibrils reveal narrow resonances indicative of a high level of microscopic sample homogeneity that permitted resonance assignments of all five species. We observed variations in chemical shift among the three dominant forms of the fibrils which were indicated by the presence of three distinct, self-consistent sets of correlated NMR signals. Similarly, the monoclinic and orthorhombic crystals exhibit chemical shifts that differ from one another and from the fibrils. Collectively, the chemical shift data suggest that the peptide assumes five conformations in the crystals and fibrils that differ from one another in subtle but distinct ways. This includes variations in the mobility of the aromatic Tyr ring. The data also suggest that various structures assumed by the peptide may be correlated to the "steric zipper" observed in the monoclinic crystals.

Introduction

Amyloidosis, or the class of disorders associated with amyloid formation, continues to attract the attention of researchers from a wide variety of scientific disciplines. These studies are of great medical importance as a key to understanding human diseases[1] and are also of considerable scientific interest, potentially providing broader insights into fundamental biological processes such as protein (mis)folding. Unfortunately, the molecular structures of the proteinaceous aggregates, from which the name of the group is derived, remain elusive despite substantial ongoing efforts. The essential biophysical characteristics of amyloid fibrils complicate their structural characterization via conventional methods of structural biology, X-ray crystallography, and solution NMR, since these techniques require either crystallization or dissolution of the material of interest.

For this reason, various complementary techniques are being applied to obtain insights into the mechanism behind the formation and structure of fibrillar aggregates.[2,3] These studies often involve truncated fragments of amyloidogenic proteins and are aimed at developing convenient model systems that yield detailed structural data. One such system is the yeast protein Sup35p which normally functions as a translation termination factor.[4−6] However, an aggregated form has been found to be the causative agent in the transmission of a phenotype [PSI(+)].[7−9] The protein is the factor leading to an inheritable phenotype that could also be induced by the introduction of preformed aggregates.[8] This is analogous to the role of the prion component in human prion disorders, a class of diseases characterized by the self-propagation of pathogenic amyloid aggregates.[10] The protein's prion-forming domain is characterized by a high percentage of glutamine and asparagine residues, similar to a class of amyloid-forming proteins implicated in various human diseases including Huntington's disease and spinal and bulbar muscular atrophy.[11] Due to the relative convenience of the yeast organism, the Sup35p protein provides an easily accessible model system for the study of this class of disorders specifically and amyloid-forming proteins in general.[12]

(1) Westermark, P. *FEBS J.* **2005**, *272*, 5942−5949.
(2) Makin, O. S.; Serpell, L. C. *FEBS J.* **2005**, *272*, 5950−5961.
(3) Tuite, M. F. *Cell* **2000**, *100*, 289−292.
(4) Hawthorne, D. C.; Mortimer, R. K. *Genetics* **1968**, *60*, 735−742.
(5) Inge-Vechtomov, S. G.; Andrianova, V. M. *Genetika* **1970**, *6*, 103−115.
(6) Stansfield, I.; Jones, K. M.; Kushnirov, V. V.; Dagkesamanskaya, A. R.; Poznyakovski, A. I.; Paushkin, S. V.; Nierras, C. R.; Cox, B. S.; Teravanesyan, M. D.; Tuite, M. F. *EMBO J.* **1995**, *14*, 4365−4373.
(7) Wickner, R. B. *Science* **1994**, *264*, 566−569.
(8) Patino, M. M.; Liu, J. J.; Glover, J. R.; Lindquist, S. *Science* **1996**, *273*, 622−626.
(9) Sparrer, H. E.; Santoso, A.; Szoka, F. C., Jr.; Weissman, J. S. *Science* **2000**, *289*, 595−599.
(10) Prusiner, S. B. *Science* **1997**, *278*, 245−251.
(11) Yamada, M.; Shimohata, M.; Sato, T.; Tsuji, S.; Takahashi, H. *Neuropathology* **2006**, *26*, 346−351.
(12) Glover, J. R.; Kowal, A. S.; Schirmer, E. C.; Patino, M. M.; Liu, J. J.; Lindquist, S. *Cell* **1997**, *89*, 811−819.

Since its identification as a prion-protein,[8] this 685-residue protein has been studied extensively,[13−20] and it was generally established that the N-terminal segment of 123 amino acids is the prion-forming domain (PrD).[8] The PrD displays a high level of amino acid degeneracy in its primary sequence, with just four residues—Gln, Asn, Tyr, and Gly—accounting for 78% of its length.[3,8] Various subsections of the PrD segment have been studied in a search for domains that are the cause, or at least share the feaures, of the fibril formation displayed by the larger protein.[21−24] Eisenberg and co-workers identified a short section from the PrD domain, residues 7−13 (GNNQQNY), as one of the shortest segments that forms fibrils exhibiting physicochemical properties similar to those found for the protein's fibrils.[25] They reported that the fibrils formed from this peptide resembled the protein fibrils in their fibrillization behavior, X-ray diffraction, and binding of Congo red. In addition, the same peptide is also able to form microcrystals that share some of the characteristics of the fibrils, and using a newly developed microcrystal diffractometer, the X-ray structure of the monoclinic crystals was determined.[26] Interestingly, the peptide also forms orthorhombic crystals that were the focus of earlier reports.[25,27] Various features of the monoclinic crystal structure were proposed to be common to both the crystals and the fibrils and even proposed to reflect general features of prion fibril formation and structure.

The X-ray structure reveals parallel β-strands that are stacked in register into β-sheets, along the longest dimension of the elongated crystals. The parallel stacked arrangement allows for strong interactions between the identical residues in neighboring strands involving 11 hydrogen bonds: backbone−backbone H-bonding, as well as Asn−Asn and Gln−Gln side-chain H-bonding. This arrangement is reminiscent of a parallel version of the polyglutamine polar zipper[28,29] and the asparagine ladders found in parallel β-helix proteins.[30,31] Another feature in common with parallel β-helix proteins[32] is the stacking of Tyr side chains, in a manner allowing favorable $\pi-\pi$ stacking interactions leading to β-sheet stabilization.[33,34] Two β-sheets are tied together by strong steric interactions with one another, due to tightly packed Asn and Gln side chains on one face of the sheets, forming a *dry interface*. This closely packed interface featuring interdigitated, structurally complementary side chains was referred to as a *steric zipper*. It was suggested to be a key feature in the formation of the peptide fibrils and a general mechanism in various other amyloid systems.[26,35,36] Its formation would require a complementary structural motif in the two "mating" surfaces. In contrast, the so-called *wet interface* features only a few direct contacts between the β-sheets, which are separated from one another by multiple water molecules, except for direct tyrosine side-chain interactions. The proximity and alignment of these Tyr rings seems to allow $\pi-\pi$ stacking interactions between the β-sheets, in addition to the Tyr−Tyr stacking within each sheet. The potential implications of these crystals' characteristics for prion fibril characterization have led to a number of experimental and theoretical studies into this peptide's characteristics.[37−41]

The reported formation of multiple crystallographic and fibrillar forms of GNNQQNY reflects a common observation in studies on amyloidogenic systems. Like many other amyloid fibrils, the Sup35p fibrils display a certain level of structural polymorphism, which appears to correlate to the existence of different strains of amyloid-related disorders in vivo.[42−44] The fact that the interstack assembly relies on a steric zipper, which does not necessarily require a high sequence specificity and could result in slightly different arrangements given the same primary sequence, has been proposed as a potential explanation for the polymorphism.[26] While Nelson et al. did not discuss the potential for polymorphism due to variations in the so-called wet interface, it seems likely that even similarly assembled steric zippers (consisting of two β-sheets) can assemble in different ways as a result of rearrangements in the interactions on that face.

An obvious first step in the examination of these proposed generalizations would be to determine the extent to which the structure found in these crystals does or does not represent the fold in the fibrils formed by the same peptide, in order to eventually compare it to larger sections of the PrD domain of Sup35p. The crystals display a number of physicochemical amyloid-like characteristics, for instance the cross-β X-ray scattering pattern and the binding of specific chromophores. Here we present a more detailed comparison of the structural features of the crystals and fibrils formed by these peptides, through investigations utilizing solid-state nuclear magnetic resonance (SSNMR). Magic angle spinning (MAS) spectra have been employed in studies of other peptide-based fibrils derived from the amyloids transthyretin, Aβ, and various other systems.[45−62] This technique is applicable to a wide variety

(13) Baxa, U.; Taylor, K. L.; Steven, A. C.; Wickner, R. B. *Contrib. Microbiol.* **2004**, *11*, 50−71.
(14) Dobson, C. M. *Nature* **2005**, *435*, 747−9.
(15) Fernandez-Bellot, E.; Cullin, C. *Cell. Mol. Life Sci.* **2001**, *58*, 1857−1878.
(16) Serio, T. R.; Lindquist, S. L. *Adv. Protein Chem.* **2001**, *59*, 391−412.
(17) Shorter, J.; Lindquist, S. *Nat. Rev. Genet.* **2005**, *6*, 435−450.
(18) True, H. L. *Trends Genet.* **2006**, *22*, 110−117.
(19) Bousset, L.; Melki, R. *Microbes Infect.* **2002**, *4*, 461−469.
(20) Ross, E. D.; Minton, A.; Wickner, R. B. *Nat. Cell Biol.* **2005**, *7*, 1039−44.
(21) Parham, S. N.; Resende, C. G.; Tuite, M. F. *EMBO J.* **2001**, *20*, 2111−9.
(22) Shkundina, I. S.; Kushnirov, V. V.; Tuite, M. F.; Ter-Avanesyan, M. D. *Genetics* **2006**, *172*, 827−35.
(23) Osherovich, L. Z.; Cox, B. S.; Tuite, M. F.; Weissman, J. S. *PLoS Biol.* **2004**, *2*, E86.
(24) Narayanan, S.; Walter, S.; Reif, B. *ChembioChem* **2006**, *7*, 757−765.
(25) Balbirnie, M.; Grothe, R.; Eisenberg, D. S. *Proc. Natl. Acad. Sci. U.S.A.* **2001**, *98*, 2375−80.
(26) Nelson, R.; Sawaya, M. R.; Balbirnie, M.; Madsen, A. O.; Riekel, C.; Grothe, R.; Eisenberg, D. *Nature* **2005**, *435*, 773−778.
(27) Diaz-Avalos, R.; Long, C.; Fontano, E.; Balbirnie, M.; Grothe, R.; Eisenberg, D.; Caspar, D. L. D. *J. Mol. Biol.* **2003**, *330*, 1165−1175.
(28) Perutz, M. F.; Staden, R.; Moens, L.; De Baere, I. *Curr. Biol.* **1993**, *3*, 249.
(29) Perutz, M. *Protein Sci.* **1994**, *3*, 1629−1637.
(30) Yoder, M. D.; Keen, N. T.; Jurnak, F. *Science* **1993**, *260*, 1503.
(31) Steinbacher, S.; Seckler, R.; Miller, S.; Steipe, B.; Huber, R.; Reinemer, P. *Science* **1994**, *265*, 383.
(32) Jenkins, J.; Mayans, O.; Pickersgill, R. *J. Struct. Biol.* **1998**, *122*, 236.
(33) Tsai, H.-H.; Reches, M.; Tsai, C.-J.; Gunasekaran, K.; Gazit, E.; Nussinov, R. *Proc. Natl. Acad. Sci. U.S.A.* **2005**, *102*, 8174−8179.
(34) Zheng, J.; Ma, B.; Tsai, C. J.; Nussinov, R. *Biophys. J.* **2006**.
(35) Nelson, R.; Eisenberg, D. *Curr. Opin. Struct. Biol.* **2006**, *16*, 260−265.
(36) Thompson, M. J.; Sievers, S. A.; Karanicolas, J.; Ivanova, M. I.; Baker, D.; Eisenberg, D. *Proc. Natl. Acad. Sci. U.S.A.* **2006**, *103*, 4074−8.
(37) Gsponer, J.; Haberthur, U.; Caflisch, A. *Proc. Natl. Acad. Sci. U.S.A.* **2003**, *100*, 5154−5159.
(38) Chae, Y. K.; Lee, K.; Kim, Y. *Protein Pept. Lett.* **2004**, *11*, 23−8.
(39) Kim, Y.; Kim, Y.; Park, J. J.; Hwang, J. H.; Park, T. J. *Key Engineering Materials*; Trans Tech Publications: Zurich, Switzerland, 2005; Vol. 277−279, pp 67−71.
(40) Lipfert, J.; Franklin, J.; Wu, F.; Doniach, S. *J. Mol. Biol.* **2005**, *349*, 648−658.
(41) Esposito, L.; Pedone, C.; Vitagliano, L. *Proc. Natl. Acad. Sci. U.S.A.* **2006**, *103*, 11533−8.
(42) King, C. Y.; Diaz-Avalos, R. *Nature* **2004**, *428*, 319−323.
(43) Diaz-Avalos, R.; King, C. Y.; Wall, J.; Simon, M.; Caspar, D. L. D. *Proc. Natl. Acad. Sci. U.S.A.* **2005**, *102*, 10165−10170.
(44) Krishnan, R.; Lindquist, S. L. *Nature* **2005**, *435*, 765−72.
(45) Spencer, R. G. S.; Halverson, K. J.; Auger, M.; McDermott, A. E.; Griffin, R. G.; Lansbury, P. T. *Biochemistry* **1991**, *30*, 10382−10387.

Table 1. Description of the Isotopically Enriched Samples Used in This Study[a]

[U-^{13}C, 15N-GNNQ]QNY			GNN[U-^{13}C,^{15}N-QQNY]		
i.d.	isotopic labeling (%)	sample prep	i.d.	isotopic labeling (%)	sample prep
M1	100	monoclinic nanocrystal, 10 mg/mL	M3	100	monoclinic nanocrystal, 10 mg/mL
M2	25	monoclinic nanocrystal, 10 mg/mL	M4	20	monoclinic nanocrystal, 10 mg/mL
O1	30	orthorhombic nanocrystal, 2 mg/mL	O2	≈20	orthorhombic nanocrystal, 2 mg/mL
F1	100	fibrils, 20 mg/mL	F4	30	fibrils, 25 mg/mL
F2	30	fibrils, 25 mg/mL			
F3	25	fibrils + monoclinic crystal, 12 mg/mL			

[a] Samples were prepared using segmentally labeled peptides where either the N-terminus (GNNQ) or the C-terminus (QQNY) was U-^{13}C,^{15}N labeled. The samples are indicated as monoclinic (M), orthorhombic (O), or fibrillar (F), prepared at 4 °C starting from an aqueous solution at peptide concentrations as marked.

of solid samples and in principle permits structural determinations of both crystalline and fibrillar aggregates. It does not require preparation of large crystals, and a reasonable level of microscopic structural homogeneity is sufficient to obtain high-quality structural information.

Here, we use solid-state MAS NMR methods to compare nanocrystals and fibrils formed by the peptide fragment GNNQQNY$_{7-13}$. At this initial stage, we focus on the determination of the assignments of the isotropic ^{13}C and ^{15}N chemical shifts of the peptide since differences in the shifts can be used to localize and identify differences in the structural features between the aggregated forms. Structural changes affecting the chemical shifts are typically dominated by the (local) structure of the monomer (i.e., its conformation) but can also include effects due to the proximity of other peptides involved in different packing arrangements. Therefore, a comparison of these parameters provides information on the localized similarities and differences between the crystalline and fibrillar forms of the peptide. In addition, structural features such as sample homogeneity and dynamics or motional flexibility can easily be evaluated with such measurements.

Samples prepared using segmentally ^{13}C,^{15}N-labeled peptides yielded both crystalline forms and fibrillar samples in accordance with the documented polymorphic behavior of GNNQQNY.[27] Subsequently, we employed a variety of multidimensional solid-state MAS dipolar recoupling NMR techniques to compare different polymorphs of the peptide. Specifically, we deconvolved the spectra of three distinct structural forms within the fibrils and compared these to one another and to the two crystalline forms. The results provide a perspective on this array of five aggregates, allow direct comparisons among the polymorphs, and elucidate several proposed features of amyloids and their formative process.

Experimental Methods

Sample Preparation. GNNQQNY was obtained by solid-phase peptide synthesis from CS Bio Inc. (Menlo Park, CA). The peptide was prepared both without isotopic enrichment and with U-^{13}C,^{15}N-labeled amino acids from Cambridge Isotope Laboratories (Andover, MA) according to a segmental labeling scheme. The two isotopically labeled variants have labeled residues in either the first four positions ([U-^{13}C,^{15}N-GNNQ]QNY) or in the final four positions (GNN[U-^{13}C,^{15}N-QQNY]), allowing complete sequential chemical shift assignments. The peptide fragment GNNQQNY is known to form either crystals or fibrils, depending on the exact protocol used.[25−27] The general protocol involves rapid dissolution of the lyophilized peptide in water, resulting in an acidic peptide solution (pH 2−3), at a concentration of 1−25 mg/mL. Depending on concentration and treatment of the solution, the peptides form either monoclinic or orthorhombic crystals and/or fibrils. A brief description of some of the different samples prepared is contained in Table 1, with further details in the Results. The peptide crystals used for MAS NMR experiments were packed into rotors using a micro centrifuge spinning at 5500*g* (VWR Scientific, West Chester, PA). The gellike fibril samples were prepared by concentrating the fibrils by centrifugation and subsequent packing into the rotor using an ultracentrifuge at 13 000*g* (Beckman-Coulter, Fullerton, CA). Unless specifically indicated otherwise, both the crystalline and fibrillar samples were kept hydrated with excess water at all times.

Transmission Electron Microscopy. Both the fibrils and the nanocrystals were examined by transmission electron microscopy using a Philips EM410 electron microscope, as described previously.[63] The peptide crystals and fibrils were negatively stained using aqueous uranyl actetate prior to measurement. The resulting micrographs were compared to reference grid samples (Electron Microscope Sciences, Hatfield PA) to ensure accurate measurements of the peptide aggregate dimensions.

NMR Methods. (a) Nanocrystal and Fibril Assignments. NMR spectra were recorded on Cambridge Instruments spectrometers (designed by D. J. Ruben, Francis Bitter Magnet Laboratory, MIT) operating at 500, 700, or 750 MHz ^{1}H frequencies or on a Bruker Avance spectrometer operating at 900 MHz ^{1}H frequency. ^{13}C chemical shifts were referenced to aqueous DSS using external referencing via the published ^{13}C chemical shifts of adamantane.[64] ^{15}N chemical shifts

(46) Jarrett, J. T.; Costa, P. R.; Griffin, R. G.; Lansbury, P. T., Jr. *J. Am. Chem. Soc.* **1994**, *116*, 9741−9742.
(47) Griffiths, J. M.; Ashburn, T. T.; Auger, M.; Costa, P. R.; Griffin, R. G.; Lansbury, P. T., Jr. *J. Am. Chem. Soc.* **1995**, *117*, 3539−3546.
(48) Lansbury, P. T.; Costa, P. R.; Griffiths, J. M.; Simon, E. J.; Auger, M.; Halverson, K. J.; Kocisko, D. A.; Hendsch, Z. S.; Ashburn, T. T.; Spencer, R. G. S.; Tidor, B.; Griffin, R. G. *Nat. Struct. Biol.* **1995**, *2*, 990−998.
(49) Costa, P. R.; Kocisko, D. A.; Sun, B. Q.; Lansbury, P. T.; Griffin, R. G. *J. Am. Chem. Soc.* **1997**, *119*, 10487−10493.
(50) Tycko, R. *Protein Pept. Lett.* **2006**, *13*, 229−34.
(51) Tycko, R. *Q. Rev. Biophys.* **2006**, 1−55.
(52) Antzutkin, O. N.; Balbach, J. J.; Leapman, R. D.; Rizzo, N. W.; Reed, J.; Tycko, R. *Proc. Natl. Acad. Sci. U.S.A.* **2000**, *97*, 13045−13050.
(53) Antzutkin, O. N.; Balbach, J. J.; Tycko, R. *Biophys. J.* **2003**, *84*, 3326−3335.
(54) Antzutkin, O. N.; Leapman, R. D.; Balbach, J. J.; Tycko, R. *Biochemistry* **2002**, *41*, 15436−15450.
(55) Balbach, J. J.; Ishii, Y.; Antzutkin, O. N.; Leapman, R. D.; Rizzo, N. W.; Dyda, F.; Reed, J.; Tycko, R. *Biochemistry* **2000**, *39*, 13748−13759.
(56) Balbach, J. J.; Petkova, A. T.; Oyler, N. A.; Antzutkin, O. N.; Gordon, D. J.; Meredith, S. C.; Tycko, R. *Biophys. J.* **2002**, *83*, 1205−1216.
(57) Petkova, A. T.; Ishii, Y.; Balbach, J. J.; Antzutkin, O. N.; Leapman, R. D.; Delaglio, F.; Tycko, R. *Proc. Natl. Acad. Sci. U.S.A.* **2002**, *99*, 16742−16747.
(58) Jaroniec, C. P.; MacPhee, C. E.; Astrof, N. S.; Dobson, C. M.; Griffin, R. G. *Proc. Natl. Acad. Sci. U.S.A.* **2002**, *99*, 16748−16753.
(59) Jaroniec, C. P.; MacPhee, C. E.; Bajaj, V. S.; McMahon, M. T.; Dobson, C. M.; Griffin, R. G. *Proc. Natl. Acad. Sci. U.S.A.* **2004**, *101*, 711−716.
(60) Chan, J. C. C.; Oyler, N. A.; Yau, W. M.; Tycko, R. *Biochemistry* **2005**, *44*, 10669−10680.
(61) Siemer, A. B.; Ritter, C.; Steinmetz, M. O.; Ernst, M.; Riek, R.; Meier, B. H. *J. Biomol. NMR* **2006**, *34*, 75−87.
(62) Ritter, C.; Maddelein, M. L.; Siemer, A. B.; Luhrs, T.; Ernst, M.; Meier, B. H.; Saupe, S. J.; Riek, R. *Nature* **2005**, *435*, 844−8.
(63) van der Wel, P. C. A.; Hu, K. N.; Lewandowski, J.; Griffin, R. G. *J. Am. Chem. Soc.* **2006**, *128*, 10840−10846.

were referenced to liquid ammonia, via indirect referencing using the suggested IUPAC frequency ratios ($^{13}C/^{1}H$) of aqueous DSS and liquid NH_3 ($^{15}N/^{1}H$).[65,66] Experiments at 500 MHz utilized Varian triple-resonance probes equipped with 4-mm stators (Revolution NMR, Fort Collins, CO), spinning at 10−12 kHz regulated to ±2 Hz with a Bruker spinning frequency controller (Bruker BioSpin, Billerica MA). At 700 and 750 MHz Varian and custom designed probes were used, respectively, using 3.2 mm rotors (Varian, Inc., and Revolution NMR, Fort Collins, CO) and MAS spinning rates of 15−20 kHz. Experiments at 900 MHz used a Bruker triple resonance probe equipped with 2.5 mm spinner module and a spinning rate of ∼20 kHz. The sample temperature was maintained by using a stream of cooled, 1 °C nitrogen gas.

1D ^{13}C MAS spectra were recorded with ramped cross-polarization (CP), using a 2 ms contact time and 100 kHz TPPM ^{1}H decoupling[67] during acquisition. The 2D $^{13}C-^{13}C$ spin diffusion experiments used a 10−12 ms mixing time, during which a ^{1}H rf field matching the $n = 1$ rotary resonance condition[68] was used to facilitate efficient $^{13}C-^{13}C$ magnetization transfer (DARR/RAD mixing).[69−72] $^{13}C-^{13}C$ correlation experiments using SPC5 mixing[73] were performed at 10 kHz MAS using a 1.5 ms mixing time with $\omega_{1C}/2\pi = 50$ kHz and $\omega_{1H}/2\pi = 100$ kHz in the form of CW decoupling. $^{13}C-^{13}C$ recoupling experiments at 900 MHz and $\omega_r/2\pi = 20$ kHz utilized cosine modulation rotary resonance,[74] CM_4RR, with a mixing period of 796 μs, $(\omega_1/2\pi)_{13C} = 84.6$ kHz, and no ^{1}H irradiation during mixing.

$^{15}N-^{13}C$ correlations were obtained through a series of double CP-based measurements.[75,76] NCA and NCO spectra[77−79] were recorded using $^{1}H-^{15}N$ CP followed by ^{15}N chemical shift evolution and band-selective specific CP resulting in selective transfer of the ^{15}N magnetization to directly bonded ^{13}CO or $^{13}C_\alpha$ by placing the ^{13}C carrier frequency in the middle of the CO (for NCO transfer) and C_α (for NCA transfer) regions. The ^{15}N radio frequency field strength was 5−20 kHz, the ^{13}C field was ramped linearly through the $n = 1$ Hartmann−Hahn matching condition, and the DCP contact time was 3 ms. 2D $^{15}N-^{13}C-^{13}C$ spectra were recorded by using the NCOCX and NCACX[80] pulse sequences that included a 10−20 ms DARR/RAD period to establish the intraresidue $^{13}C-^{13}C$ correlations. Unless otherwise noted, the NMR spectra of the fibrils were acquired in essentially the same manner as the crystals.

(b) NMR Data Analysis. NMR data processing and assignment were done with the aid of the NMRPipe[81] and Sparky[82] software packages.

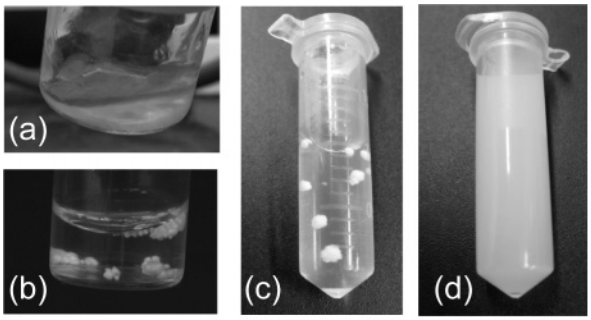

Figure 1. Photographs of various GNNQQNY aggregates: (a) fibrils prepared at 25 mg/mL; (b) clusters of monoclinic crystals at 10 mg/mL after filtration; (c) monoclinic crystals imbedded in fibril gel at 10 mg/mL (no filtration); (d) a suspension of orthorhombic crystals obtained after swirling a 2 mg/mL solution.

Analysis of the peptide backbone (and C_β) chemical shifts was performed using the TALOS software (version 2003.027.13.05),[83] using the default database of 78 proteins. The N-terminal nitrogen and C-terminal carbonyl atoms were excluded from this analysis. Secondary shift calculations[84,85] were performed by subtracting the random coil shifts listed by Zhang et al.[86]

Results

Peptide Aggregate Preparation. The type of aggregates formed by GNNQQNY can be controlled by seeding with preformed aggregates and other variations in the sample preparation protocol, with the most notable differentiation dependent on the peptide concentration.[27] To illustrate the appearance of our samples, we show in Figure 1 photographs of the different aggregated forms. The formation of fibrils was predominantly observed at higher peptide concentrations, when dissolving the peptide at 10−25 mg/mL, followed by fibrillization for 2−3 days at 4 °C or room temperature. This yielded a highly viscous gellike sample, as illustrated in Figure 1a. In contrast, near 10 mg/mL the peptide has a tendency to form the monoclinic nanocrystals previously studied by X-ray diffraction.[26] These monoclinic crystals form typical snowball-like clusters as seen in Figure 1b,c. At this concentration, the sample often contains both the snowball-like crystals and gellike fibrils (Figure 1c), unless one uses rapid filtration using 0.2 μm filters to remove initial fibrillization sources (Figure 1b). The fibril formation at higher peptide concentrations is unaffected by filtration of the solution. In our experiments, at low concentrations (1−2 mg/mL) the formation of fibrils is suppressed, but after several days at 4 °C the formation of monoclinic crystals was observed even in the absence of filtration. If these low concentration peptide solutions are swirled during crystallization, the formation of crystals is accelerated, but the spherical clusters are not observed. Rather, one obtains white suspensions (Figure 1d) that, under seemingly identical conditions, comprise either the monoclinic crystals[26] or the orthorhombic crystal form reported in earlier literature.[25,27] In general, we note that there was some level of variability in the

(64) Morcombe, C. R.; Zilm, K. W. *J. Magn. Reson.* **2003**, *162*, 479−486.
(65) Markley, J. L.; Bax, A.; Arata, Y.; Hilbers, C. W.; Kaptein, R.; Sykes, B. D.; Wright, P. E.; Wüthrich, K. *Pure Appl. Chem.* **1998**, *70*, 117−142.
(66) Harris, R. K.; Becker, E. D.; Cabral de Menezes, S. M.; Goodfellow, R.; Granger, P. *Solid State Nucl. Magn. Reson.* **2002**, *22*, 458−483.
(67) Bennett, A. E.; Rienstra, C. M.; Auger, M.; Lakshmi, K. V.; Griffin, R. G. *J. Chem. Phys.* **1995**, *103*, 6951−6957.
(68) Oas, T. G.; Griffin, R. G.; Levitt, M. H. *J. Chem. Phys.* **1988**, *89*, 692−695.
(69) Takegoshi, K.; Nakamura, S.; Terao, T. *Chem. Phys. Lett.* **2001**, *344*, 631−637.
(70) Takegoshi, K.; Nakamura, S.; Terao, T. *J. Chem. Phys.* **2003**, *118*, 2325−2341.
(71) Morcombe, C. R.; Gaponenko, V.; Byrd, R. A.; Zilm, K. W. *J. Am. Chem. Soc.* **2004**, *126*, 7196−7197.
(72) Costa, P. R.; Veshtort, M.; Griffin, R. G. *ENC Conf. Abstr.* **1998**, Poster No. 156.
(73) Hohwy, M.; Rienstra, C. M.; Jaroniec, C. P.; Griffin, R. G. *J. Chem. Phys.* **1999**, *110*, 7983−7992.
(74) De Paepe, G.; Bayro, M. J.; Lewandowski, J.; Griffin, R. G. *J. Am. Chem. Soc.* **2006**, *128*, 1776−1777.
(75) Schaefer, J.; Mckay, R. A.; Stejskal, E. O. *J. Magn. Reson.* **1979**, *34*, 443−447.
(76) Stejskal, E. O.; Schaefer, J.; Mckay, R. A. *J. Magn. Reson.* **1984**, *57*, 471−485.
(77) Baldus, M.; Petkova, A. T.; Herzfeld, J.; Griffin, R. G. *Mol. Phys.* **1998**, *95*, 1197−1207.
(78) Petkova, A. T.; Baldus, M.; Belenky, M.; Hong, M.; Griffin, R. G.; Herzfeld, J. *J. Magn. Reson.* **2003**, *160*, 1−12.
(79) Egorova-Zachernyuk, T. A.; Hollander, J.; Fraser, N.; Gast, P.; Hoff, A. J.; Cogdell, J.; de Groot, H. J. M.; Baldus, M. *J. Biomol. NMR* **2001**, *19*, 243−253.
(80) Pauli, J.; Baldus, M.; van Rossum, B.-J.; de Groot, H. J. M.; Oschkinat, H. *Chembiochem* **2001**, *2*, 272−281.
(81) Delaglio, F.; Grzesiek, S.; Vuister, G. W.; Zhu, G.; Pfeifer, J.; Bax, A. *J. Biomol. NMR* **1995**, *6*, 277−293.
(82) Goddard, T. D.; Kneller, D. G. *SPARKY*, 3rd ed.; University of California: San Francisco, CA, 2006.
(83) Cornilescu, G.; Delaglio, F.; Bax, A. *J. Biomol. NMR* **1999**, *13*, 289−302.
(84) Wishart, D. S.; Sykes, B. D.; Richards, F. M. *J. Mol. Biol.* **1991**, *222*, 311−33.
(85) Wishart, D. S.; Nip, A. M. *Biochem. Cell Biol.* **1998**, *76*, 153−63.
(86) Zhang, H.; Neal, S.; Wishart, D. S. *J. Biomol. NMR* **2003**, *25*, 173.

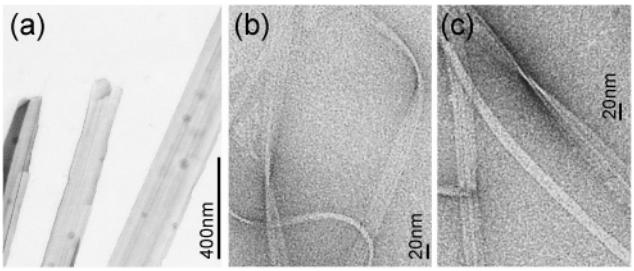

Figure 2. Transmission electron micrograph images of GNNQQNY (a) monoclinic nanocrystals obtained at 10 mg/mL and (b, c) fibrillar aggregates formed at 25 mg/mL.

result of the different protocols, especially in the size of the crystals and the relative amounts of fibrils and crystals.

Monoclinic Nanocrystal Characterization. We first focus our attention on the monoclinic crystals for which an X-ray structure exists.[26] Figure 2a shows a transmission electron micrograph of typical crystallites making up the spherical aggregates shown in Figure 1b,c.

TEM data acquired for crystals from a number of different samples revealed an average crystal width of ~150−200 nm but with much longer lengths, of the order of micrometers. These dimensions are consistent with the monoclinic crystal size described in the literature.[26] ^{13}C MAS spectra from natural abundance nanocrystals yielded spectra with very narrow line widths, indicative of a high level of homogeneity and uniformity (Figure 3a). However, as judged by their line widths, the homogeneity of different monoclinic preparations varied slightly but reproducibly yielded a single and identical set of chemical shifts. The 1D ^{13}C spectrum in Figure 3a was obtained at 750 MHz (^{1}H frequency) and illustrates the narrow line widths achievable with natural abundance samples (ranging from 31 to 52 Hz or 0.16−0.28 ppm).

Figure 3a also shows the assignments of the ^{13}C resonances obtained using two segmentally labeled peptides, prepared by solid-phase peptide synthesis. The peptides were uniformly ^{13}C,^{15}N-labeled in the first four or last four residues of the heptapeptide: [U-^{13}C,^{15}N-GNNQ]QNY and GNN[U-^{13}C,^{15}N-QQNY]. Each peptide was used to prepare both 100%-labeled and isotopically dilute (20−30%-labeled) samples. One-dimensional ^{13}C and ^{15}N spectra for both peptides are shown in Figure 4 (panels a and b). The resonance frequencies are reproducible between samples and the ^{13}C frequencies match the earlier results from unlabeled peptide. The line widths (0.8−1.0 ppm for ^{13}C, 1.0−1.3 ppm for ^{15}N) are increased due to the presence of ^{13}C−^{13}C *J*-couplings and variations in sample homogeneity.

Several 2D experiments were performed on these samples to establish connectivity patterns and determine the specific resonance assignments. An overview of the results is included as Figure 5. The pulse sequences employed include standard heteronuclear experiments such as NCA, NCO, NCOCX, and homonuclear experiments relying on SPC5 and DARR/RAD mixing (see Methods).

These 2D spectra were sufficient to unequivocally assign each of the observed resonances, and the shifts and the respective assignments are tabulated in Table 2. The ^{13}C shifts are based on the natural abundance, high-field spectra, giving a typical standard deviation of 0.05−0.1 ppm, while the isotopically enriched samples were used to obtain the ^{15}N resonances with a standard deviation of 0.1−0.2 ppm. As was apparent from the natural abundance spectra, the ^{13}C resonances generally show good dispersion, but the overlap of the ^{15}N chemical shifts is significant. This result is not unexpected given the repetitive sequence of the peptide (three N's and two Q's) and the fact that its secondary structure is entirely β-sheet.

The chemical shifts obtained here can be indexed relative to averaged random coil shifts[86,87] to obtain a preliminary identification of the secondary structure. The results of such an analysis are shown in Figure 6 and indicate the expected β-sheet character typical of amyloid structures. Additionally, one can use the chemical shift analysis program TALOS[83] to estimate the peptide backbone angles. The results of such an analysis are listed in Table 3, which includes the same torsion angles obtained from the crystal structure.[26] As expected, the chemical shifts are found to be consistent with the β-sheet structure. We note that TALOS has been used to analyze the structure of transthyretin amyloid fibrils (WT TTR 105−115) that contain exclusively β-sheet secondary structure. Further, in that study the TALOS results were compared with direct measurements of the torsion angles using dipolar recoupling experiments. The error bars and discrepancies in the TALOS fits, in the experimental measurements, and the differences between the two data sets were, with some exceptions, ~15−20°. This is the size errors that we see in Table 3, and therefore, we consider the TALOS angles quite reasonable.

Orthorhombic Crystals. Previous publications on crystals obtained for GNNQQNY have described two different crystal forms: earlier papers[25,27] focused on an orthorhombic form, whereas more recent data[26] are for the monoclinic crystals described above. In our preparations, we typically encounter the monoclinic crystals but also prepared some orthorhombic samples. Initial preparation involved a low concentration of peptide (2 mg/mL), which was swirled overnight. While seemingly identical conditions also yielded monoclinic crystals in other trials, we used seeding of the solution with existing crystals to control the crystal form made. Figure 3b shows the ^{13}C 1D spectrum of this crystal form, in which it is clear that there are significant differences from the equivalent monoclinic sample in panel a (note that this is a weakly labeled sample containing about 3% [U-^{13}C,^{15}N-GNNQ]QNY peptide, as a result of seeding the crystallization). Again, the same segmentally ^{13}C and ^{15}N labeled peptides were used to obtain full assignments of the ^{13}C and ^{15}N resonances (1D ^{13}C and ^{15}N spectra in Figure 4). Note that the measurements for the orthorhombic crystals were done at higher field and higher spinning frequencies, resulting in improved line widths (0.6−0.8 ppm for ^{13}C, 0.7−0.9 ppm for ^{15}N) compared to the monoclinic crystal data discussed earlier. The chemical shifts are largely similar to the monoclinic crystals but do show significant changes in a number of positions. A more detailed description of the various changes follows in a later section. One of the more remarkable and obvious differences concerns the aromatic resonances of the Tyr side chain. In the spectra obtained from the monoclinic crystals, these resonances are all clearly distinguishable, suggesting a rigid, immobile aromatic ring. However, as can be seen in Figures 3 and 4c, the aromatic intensities for the unlabeled Tyr signals in the spectra of the orthorhombic crystals are significantly reduced, with the $C_{\delta 1}$/

(87) Wishart, D. S.; Sykes, B. D. *J. Biomol. NMR* **1994**, *4*, 171−80.

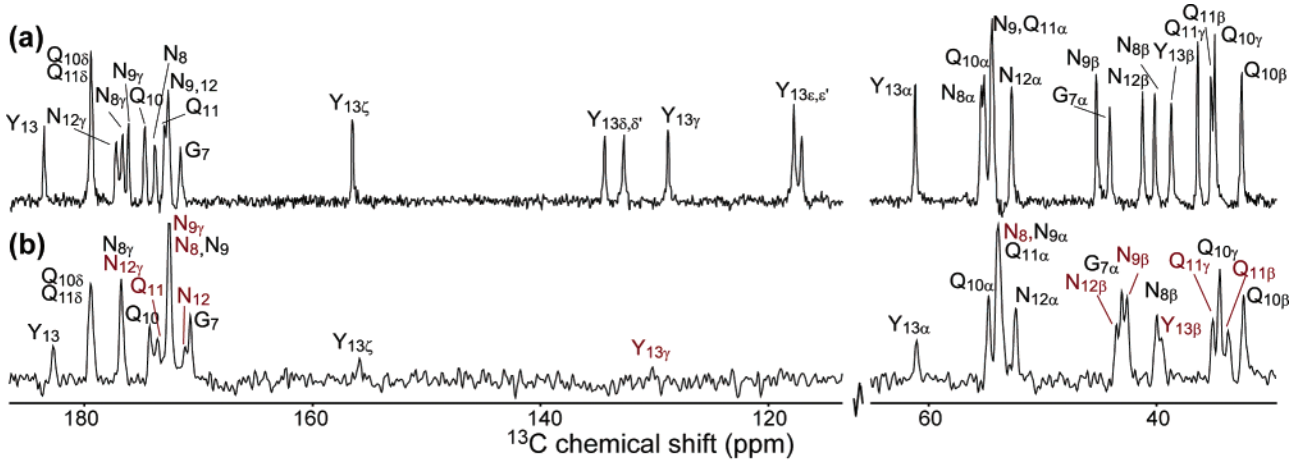

Figure 3. ^{13}C 1D spectra of natural abundance (a) monoclinic nanocrystals and (b) isotopically dilute (~3% segmentally labeled in GNNQ$_{7-10}$) orthorhombic nanocrystals of GNNQQNY. Spectra were acquired at 750 and 700 MHz ^{1}H frequencies, respectively. Red labels indicate sites displaying the most significant change in chemical shift between the two forms.

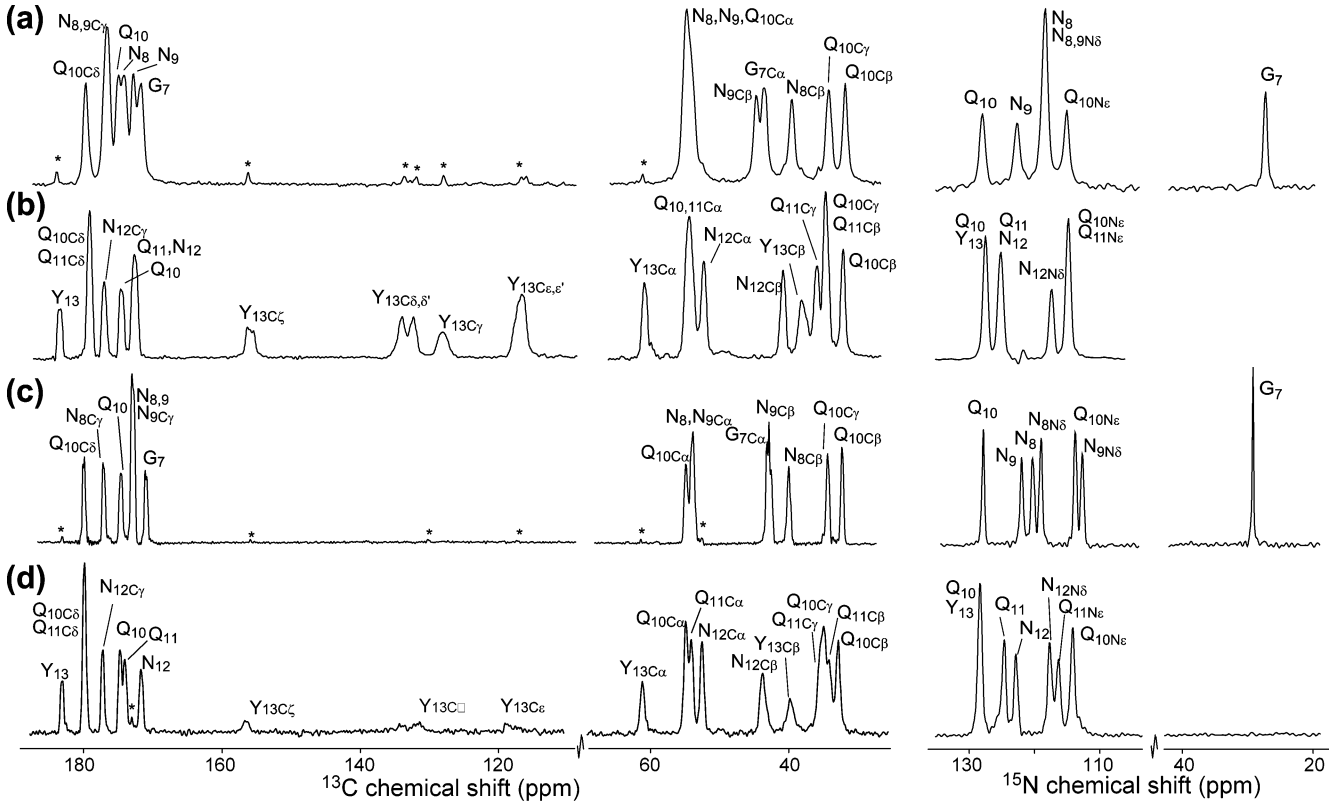

Figure 4. 1D ^{13}C and ^{15}N spectra of (a, b) monoclinic and (c, d) orthorhombic GNNQQNY nanocrystals, obtained at 500 MHz and 700 MHz ^{1}H fields, respectively. Rows a and c are for labeled [U-^{13}C,^{15}N-GNNQ]QNY samples M2 and M3, while rows b and d are labeled GNN[U-^{13}C,^{15}N-QQNY] O1 and O2.

$C_{\delta 2}$ and $C_{\epsilon 1}/C_{\epsilon 2}$ pairs now each degenerate in their chemical shift. These features suggest that the aromatic ring is executing 2-fold flips at an intermediate exchange rate that results in two effects. First, the motion averages the $C_{\delta 1}/C_{\delta 2}$ and $C_{\epsilon 1}/C_{\epsilon 2}$ chemical shifts, and second, the flipping rate tends to be near to the frequencies of the decoupling/ cross polarization rf fields and interfere with the efficiency of these two processes.[88,89] The latter primarily results in an attenuation of the intensity of the aromatic ^{13}C lines rather than a line broadening.[88] A similar loss of intensity for the tyrosine aromatic rings was observed in ^{13}C spectra of WT transthyretin (TTR 105−115) peptides.[58,59] Further, this type of motion is well documented as being present in small peptides and proteins and has been studied by ^{2}H NMR.[90,91] Another interesting observation is that spectra of the GNN[U-^{13}C,^{15}N-QQNY] ^{13}C sample initially showed signals due to a trace amount of monoclinic crystal that formed despite

(88) Long, J. R.; Sun, B. Q.; Bowen, A.; Griffin, R. G. *J. Am. Chem. Soc.* **1994**, *116*, 11950−11956.
(89) Maus, D. C.; Copié, V.; Sun, B.; Griffiths, J. M.; Griffin, R. G.; Luo, S.; Schrock, R. R.; Liu, A. H.; Seidel, S.; Davis, W. M.; Grohmann, A. *J Am. Chem. Soc.* **1996**, *118*, 5665−5671.
(90) Rice, D. M.; Wittebort, R. J.; Griffin, R. G.; Meirovich, E.; Stimson, E. R.; Meinwald, Y. C.; Freed, J. H.; Scheraga, H. A. *J. Am. Chem. Soc.* **1981**, *103*, 7707.
(91) Rice, D. M.; Meinwald, Y. C.; Scheraga, H. A.; Griffin, R. G. *J. Am. Chem. Soc.* **1987**, *109*, 1636.

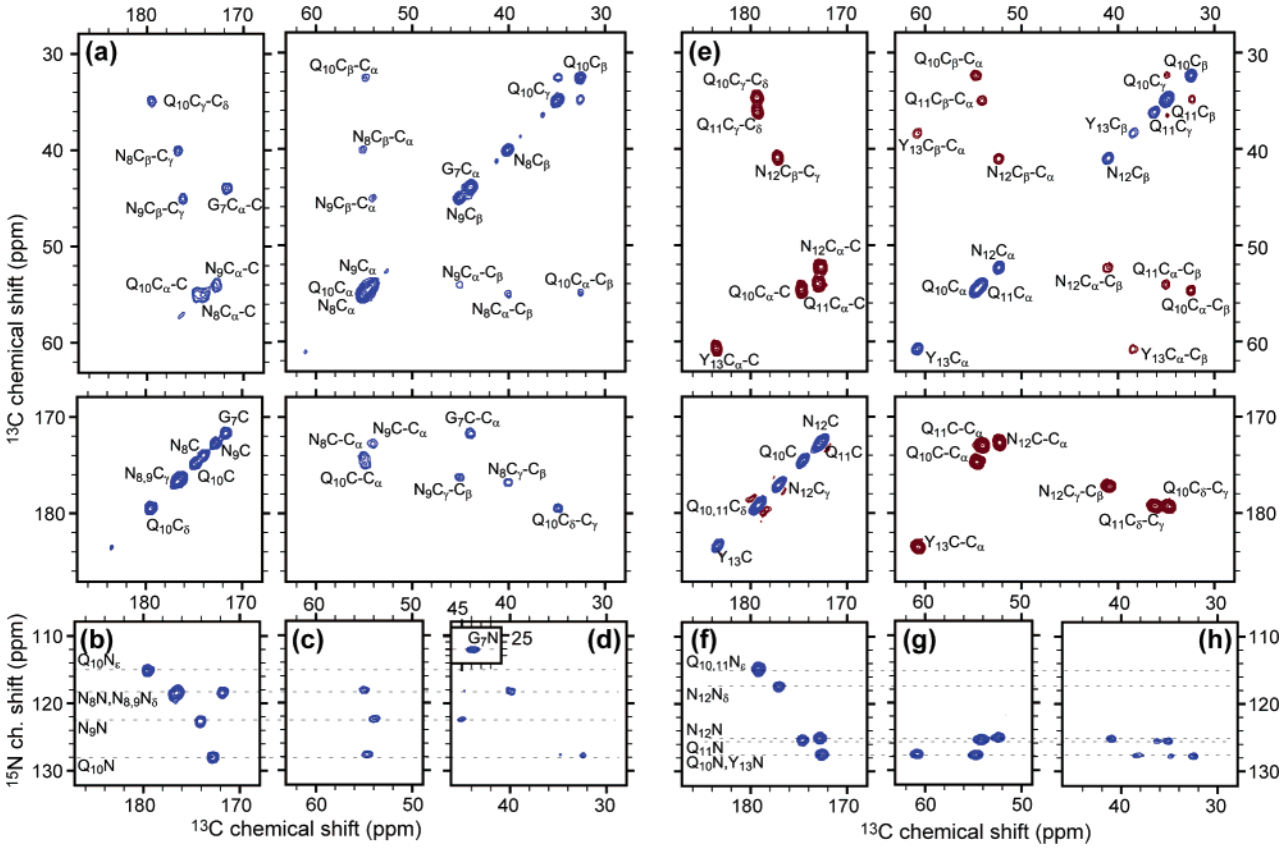

Figure 5. 2D assignment data for monoclinic crystal samples of [U-^{13}C,^{15}N-GNNQ]QNY (sample M2, panels a−d) and GNN[U-^{13}C,^{15}N-QQNY] (M3, panels e−f). The data were obtained at 500 MHz ^{1}H frequency and 10 kHz MAS. ^{13}C−^{13}C correlations (a, e) were obtained via DARR/RAD and SPC5 mixing, respectively. ^{15}N−^{13}C correlations were obtained in NCO (b, f), NCA (c, g), and NCACX experiments (d, h).

Table 2. Chemical Shifts of the Nuclei in Monoclinic Nanocrystals of GNNQQNY[a]

	^{13}C chem shift (ppm)									^{15}N chem shift (ppm)		
residue	C′	C_α	C_β	C_γ	C_δ	$C_{\delta'}$	C_ϵ	$C_{\epsilon'}$	C_ξ	N	N_δ	N_ϵ
Gly_7	171.46	43.92								27.0		
Asn_8	173.64	55.08	40.02	176.54						118.0	118.0	
Asn_9	172.58	54.21	45.10	176.01						122.2	118.0	
Gln_{10}	174.56	54.98	32.43	34.81	179.25					127.7		114.8
Gln_{11}	172.68	54.21	35.10	36.25	179.25					125.4		114.8
Asn_{12}	172.58	52.57	41.11	177.08						125.4	117.5	
Tyr_{13}	183.35	60.93	38.58	128.94	134.50	132.81	117.99	117.32	156.46	127.7		

[a] The listed ^{13}C frequencies are based on natural abundance spectra and have an uncertainty of 0.05−0.1 ppm. The ^{15}N frequencies are based on ^{15}N-enriched samples and have an uncertainty of ∼0.2 ppm. ^{13}C chemical shifts are referenced relative to DSS and ^{15}N chemical shifts are referenced relative to liquid NH_3, according to IUPAC6[5,66] using indirect referencing based on adamantane.[64]

seeding with orthorhombic material. However, successive spectra recorded from the same sample indicated a reduction of the amount of monoclinic crystals, which apparently spontaneously converted to the orthorhombic form.

The results of the assignment experiments are included in the Supporting Information for this article, with selected sections shown in figures in the paragraphs below. The assignments and chemical shifts are listed in Table 4. We also show the secondary chemical shifts in Figure 6, illustrating that the differences in the backbone chemical shifts between the two crystalline forms are small. This is also reflected in the results of a TALOS analysis included in Table 3. The only significant changes are toward the ends of the peptide, with basically no significant changes in the central residues. As will be discussed in more detail below, larger chemical shift differences are found in the side chains and are not limited to the Tyr ring dynamics mentioned earlier.

GNNQQNY Peptide Fibril Characterization. As reported previously by Diaz-Avalos et al.,[27] we find that, at higher concentrations (>10 mgs/mL), the GNNQQNY peptides tend to form fibrils. TEM micrographs (Figure 2b,c) of these samples show extended fibrils that are both significantly longer and narrower than the nanocrystals depicted in Figure 2a. The narrow fibrils have a typical width of 10−20 nm width, but there are also wider fibril aggregates of widths up to ∼50 nm. The thin striplike fibrils are tens of micrometers in length and display lengthwise striations spaced at ∼5 nm of each other. Attempts at preparing fibrils at lower concentrations, as described by Eisenberg et al.,[25,26] have as yet been unsuccessful, as also indicated by Diaz-Avalos et al.[27]

We used segmentally labeled [U-^{13}C,^{15}N-GNNQ]QNY peptide to prepare a number of fibril samples, under several different conditions, with the aim of evaluating the structural heterogeneity of these samples and allowing a qualitative comparison with

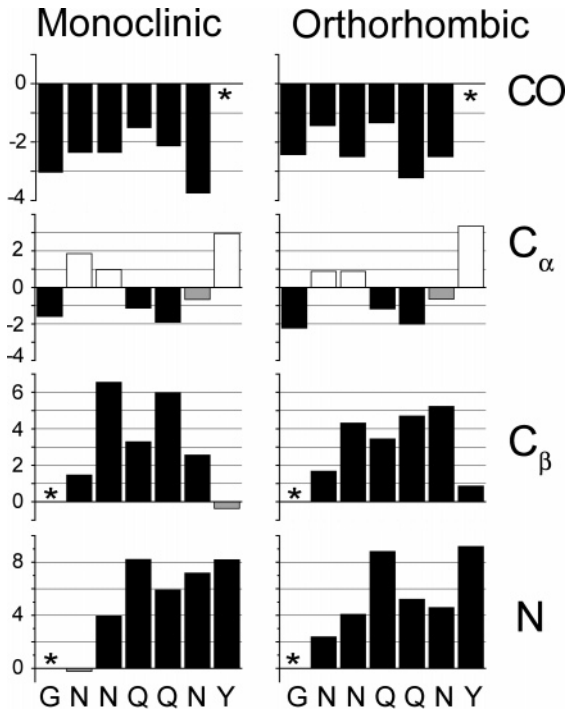

Figure 6. Secondary chemical shift for the monoclinic and orthorhombic nanocrystals. Color coding: black = β-sheet; white = α-helical; gray = indeterminate.

the crystalline forms. Using this peptide, a fully (100%, F1) and several isotopically dilute (25−30%, F2−F3) labeled samples were prepared for solid-state NMR analysis, as listed in Table 1. Figure 7 shows 1D ^{13}C and ^{15}N spectra for several of the samples, obtained with 700 MHz or 900 MHz spectrometers. The one-dimensional spectra are generally very similar, with some variations in their resolution that we attribute to heterogeneous broadening associated with variations in sample preparation. In addition, the resolution displayed by the spectra is dependent on the magnetic field and the sample spinning frequency at which the spectra were recorded with the spectrum recorded at 900 MHz and $\omega_r/2\pi = 20.161$ kHz displaying the highest resolution (sample F3; typical ^{13}C line widths of 0.6−0.8 ppm). All other fibril samples were observed at 700 MHz and $\omega_r/2\pi = 12-15$ kHz MAS (^{13}C line widths of 0.5−1.1 ppm, depending on the sample). Note that some of the narrower lines in the 900 MHz spectrum are due to coexisting monoclinic crystal signals but also that the fibril line widths are actually not much larger than those observed for the nanocrystals (0.5−0.7 ppm ^{13}C crystal line widths), suggesting that these fibril samples are quite amenable to study with SSNMR. However, when one compares these spectra to the crystalline data shown in Figure 4a,c, each of the fibril spectra displays multiple peaks for each resonance, thus limiting the amount of analysis that can be performed with 1D data. Nevertheless, one can establish that there are clear differences in chemical shifts when compared to the GNNQQNY crystals.

Two of the fibril samples (100% labeled F1 and 30% labeled F2) were used for complete resonance assignment experiments, which were performed at 700 MHz, using a number of two- and three-dimensional $^{13}C-^{13}C$ and $^{15}N-^{13}C$ correlation experiments. These experiments confirmed the presence of at least three conformations. Thus, in both samples, the spectra are dominated by three distinct sets of cross-peaks, each of which can be traced throughout the spectra. The chemical shifts for each of these fibril forms are listed in Table 5. The three different polymorphs are referred to as fibril forms 1−3, in order of the decreasing relative intensities of their spectral lines. The relative intensities varied slightly between samples, resulting in fibril 2 being the dominant polymorph in some samples. Cross-peaks due to a fourth form could sometimes be distinguished, but its concentration was too low to permit extensive study. Although we recorded 1D and 2D spectra of a sample labeled as GNN[U^{13}C,^{15}N-QQNY] (sample F4), the quality of the spectra was limited by the quantity of available material. Thus, we were not able to completely assign the spectra of this part of the peptide. Nevertheless, the spectra did permit us to determine that the Tyr ring is performing 2-fold 180° flips (vide infra).

As mentioned previously, the fact that we observe three sets of distinct chemical shifts tells us immediately that there are three distinct structures present in the form of fibrils. In Figure 8 we show the secondary shifts measured for the labeled segment within the three different fibril forms. Interestingly, one of them (fibril 2) is not entirely consistent with a pure β-sheet secondary structure, since it exhibits various secondary shifts that are more consistent with a local α-helical structure (colored white in the figure). The other two fibril forms (1 and 3) have chemical shifts indicative of the presence of β-sheet (compared to the crystal data in Figure 6, the C_α shifts are actually more strongly β-sheetlike in fibril 1 and 3). A TALOS analysis of the available chemical shifts allows one to estimate the backbone angles of Asn_8 and Asn_9. For fibril 2 we find (ϕ, ψ) angles of (54 ± 6, 40 ± 13) for Asn_8 (normally seen in left-handed α-helices) and ambiguous results for Asn_9. The other two forms do conform to a β-sheet structure, with (ϕ, ψ) angles for the Asn_8 and Asn_9 in fibril 1 of (−108 ± 20, 127 ± 10) and (−101 ± 19, 131 ± 8) and for fibril 3 of (−119 ± 18, 131 ± 12) and (−116 ± 19, 128 ± 8). Consistent with the CSI analyses, these backbone angles suggest a β-sheet structure, for both fibril forms 1 and 3, and an unspecified non-β-sheet structure for fibril 2. Note that the suggestion of "α-helical" structure in a single residue is insufficient to expect an actual α-helix to be present.

There are several reasons why it is of particular interest to examine the signals of the Tyr ring in the fibril samples. One of the major differences between the monoclinic and orthorhombic crystalline forms was found to be the dynamic behavior of the Tyr ring. Also, it has been suggested that aromatic residues may have a special role to play in the formation and/or stabilization of amyloid-like fibrils.[33,37,92] Finally, Tyr is the second-most common amino acid in the PrD domain of Sup35p. Figure 9 shows both the background natural abundance signals observed in an isotopically dilute [U-^{13}C,^{15}N-GNNQ]QNY sample (panel a) and the same signals as determined in the isotopically labeled residue (panel b). Similar to the orthorhombic crystals, some of the Tyr signals in these spectra are attenuated and lack resolved peaks for the δ,δ' and ϵ,ϵ' positions of the aromatic ring. Concurrently there is a sharp component in the spectra that suggests a population of Tyr side chains in

(92) Azriel, R.; Gazit, E. *J. Biol. Chem.* **2001**, *276*, 34156−34161.
(93) Pettersen, E. F.; Goddard, T. D.; Huang, C. C.; Couch, G. S.; Greenblatt, D. M.; Meng, E. C.; Ferrin, T. E. *J. Comput. Chem.* **2004**, *25*, 1605−1612.
(94) DeLano, W. L. *The PyMOL Molecular Graphics System*; DeLano Scientific: San Carlos, CA, 2002.

Table 3. Torsion Angle Data for the Peptide Backbone of Crystalline GNNQQNY[a]

	monoclinic crystals (NMR/TALOS)		orthorhombic crystals (NMR/TALOS)		monoclinic crystals (X-ray)	
residue	ϕ	ψ	ϕ	ψ	ϕ	ψ
Asn_8	-89 ± 17	131 ± 10	-120 ± 23	130 ± 10	-60.6	141.2
Asn_9	-139 ± 13	136 ± 9	-129 ± 19	128 ± 8	-119.2	125.2
Gln_{10}	-106 ± 17	126 ± 14	-128 ± 16	134 ± 20	-126.2	112.8
Gln_{11}	-134 ± 18	142 ± 15	-136 ± 15	143 ± 19	-115.0	126.8
Asn_{12}	-104 ± 19	119 ± 13	-135 ± 14	132 ± 16	-116.4	97.7

[a] The predicted torsion angles are based on analysis of the isotropic chemical shift values using the TALOS program.[83] Also listed are the equivalent torsion angles found in the X-ray crystal structure of the monoclinic crystals.[26]

Table 4. Chemical Shifts of the Nuclei in Orthorhombic Nanocrystals of GNNQQNY[a]

	^{13}C chem shift (ppm)									^{15}N chem. shift (ppm)		
residue	C	C_α	C_β	C_γ	C_δ	$C_{\delta'}$	C_ϵ	$C_{\epsilon'}$	C_ξ	N	N_δ	N_ϵ
Gly_7	170.86	43.28								29.2		
Asn_8	172.73	54.11	40.23	176.97						120.6	119.4	
Asn_9	172.73	54.11	42.86	172.73						122.3	113.0	
Gln_{10}	174.40	54.94	32.59	34.67	179.67					128.3		114.1
Gln_{11}	173.77	54.11	33.84	35.30	179.67					124.7		116.3
Asn_{12}	171.34	52.58	43.77	176.97						122.8	117.9	
Tyr_{13}	182.94	61.33	39.81	*130.7*	*133.1*	*133.1*	*117.7*	*117.7*	*156.0*	128.7		

[a] The resonances are based on a combination of natural abundance and labeled data. Tyr side chain resonances (in italics) are partially averaged indicating dynamics of the aromatic ring.

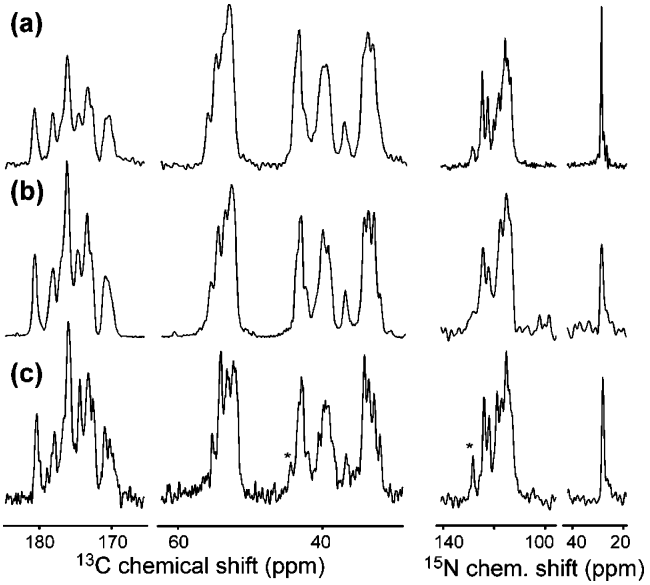

Figure 7. 1D ^{13}C and ^{15}N spectra of fibrils formed using [U-^{13}C,^{15}N-GNNQ]QNY: (a) 100%-labeled sample F1 (20 mg/mL) at 700 MHz; (b) 25%-labeled sample F2 (25 mg/mL) at 700 MHz; (c) sample F3 (12 mg/mL) at 900 MHz (contains monoclinic crystals as well (asterisk)).

the fast exchange motional limit, for which the δ,δ' and ϵ,ϵ' positions of the aromatic ring are averaged but not attenuated. Thus, in the fibrils, as well as in the orthorhombic crystals, the Tyr ring is performing 180° flips and, therefore, must not experience the same steric restrictions that prevent this motion in the monoclinic crystals. Additional experimental data on the ring dynamics for the orthorhombic crystals and each of the three fibril forms are being collected and will be reported in a future publication.

Comparison of the GNNQQNY Aggregates. We can use the experimental chemical shifts to compare the different aggregated forms observed for GNNQQNY. First, we determined the overall root-mean-square-deviation (rmsd) between the observed chemical shifts of the different forms. Table 6 compares the chemical shifts of the five GNNQQNY aggregates—the two crystalline forms and the three forms in the fibril samples—that we examined with one another. These data show that the differences between the two crystalline forms are relatively small but far from insignificant. The data also show that the three different fibril forms display a range of chemical shift deviations. When the fibril and crystal data are compared, it is fibril 3 that shows the smallest deviation relative to the monoclinic crystals, while fibrils 1 and 2 more strongly resemble each other than they resemble either crystalline polymorph.

Although the comparison of the overall rmsd is inherently approximate, it permits us to delineate the differences among the two crystal and three fibril forms in more detail by examining a few selected regions of the spectra. For example, we can compare the ^{15}N and ^{13}C═O chemical shifts present in the N−CO spectra of the different polymorphs. Some typical spectra are shown in Figure 10, with color coding of the various assignments. In the case of the two crystalline forms, the largest change is seen in the Asn_9 side chain resonances (i.e., 5 ppm change for N_δ and 3.3 ppm for C_γ of Asn_9), although several of the other cross-peaks also shift by 1−1.5 ppm. Generally larger chemical shift differences are apparent between the various fibril forms. As mentioned above, we find the largest similarities between the monoclinic crystals and fibril 3, which corresponds to the least intense signal in the different fibril samples. By far the largest changes are seen in the fibril 2, with for instance a large shift in the Gln_{10} N/Asn_9 C′ cross-peak which is due to a change of 10 ppm for the Gln_{10} backbone nitrogen and 3.4 ppm for the Asn_9 backbone carbonyl resonance. Also, its Asn_8 and Asn_9 display large changes in their ^{15}N chemical shifts (4.5−6 ppm) relative to the crystal forms. In general, we see that in particular the ^{15}N chemical shift is a very sensitive indicator of the polymorph type.

Figure 11 highlights the aliphatic ^{13}C−^{13}C cross-peaks for a number of [U-^{13}C,^{15}N-GNNQ]QNY samples. The two crystalline forms show subtle differences in chemical shift, mostly located in the Asn side chain resonances (panels a and b). From panel c it is clear that the three predominant fibril forms are particularly easy to distinguish in the Gln_{10} side chain reso-

Table 5. Assignment of Fibril Form Resonances for the Three Dominant Forms Found in 100% [U-^{13}C,^{15}N-GNNQ]QNY Fibril Sample F1[a]

		^{13}C chem shift (ppm)					^{15}N chem shift (ppm)		
	residue	C	C_α	C_β	C_γ	C_δ	N	N_δ	N_ϵ
fibril 1 (39%)	Gly7	171.2	43.5				27.6		
	Asn_8	172.8	53.0	39.7	177.3		121.1	114.0	
	Asn_9	173.5	52.7	40.4	176.4		123.0	114.5	
	Gln_{10}	176.5	55.0	34.0	34.7	180.8	123.3		114.3
fibril 2 (35%)	Gly_7	170.6	44.1				27.4		
	Asn_8	173.8	56.0	37.3	178.5		113.2	112.0	
	Asn_9	176.0	53.3	39.2	176.2		116.8	113.5	
	Gln_{10}	174.8	54.0	33.4	33.3	178.2	117.5		112.0
fibril 3 (27%)	Gly_7	170.1	43.4				27.5		
	Asn_8	174.2	52.6	40.1	177.0		118.6	115.2	
	Asn_9	173.3	53.7	42.6	176.2		121.3	115.5	
	Gln_{10}	174.8	54.7	32.5	34.2	180.8	127.1		114.5

[a] Sample F1 was prepared at 20 mg/mL. The sets of resonances labeled as 1−3 are listed alongside their estimated relative intensities in the spectra.

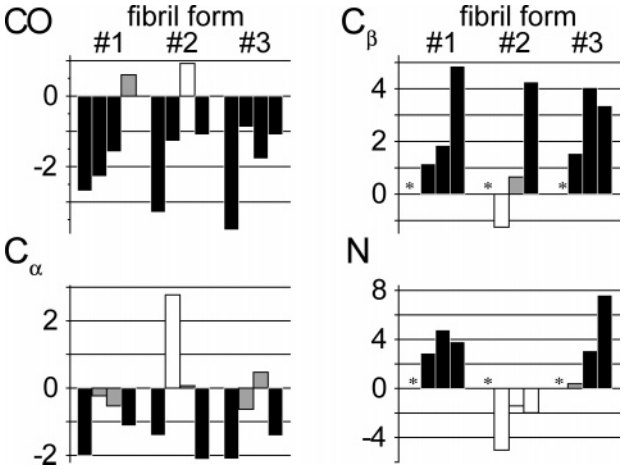

Figure 8. Secondary chemical shift analysis of $GNNQ_{7-10}$ in GNNQQNY fibril forms 1−3. Color coding: black = β-sheet; white = α-helical; gray = indeterminate.

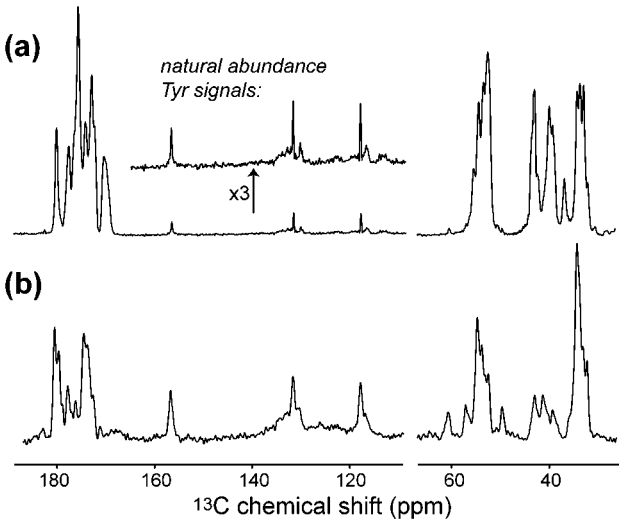

Figure 9. Tyrosine-13 in fibril samples consisting of (a) diluted [U-^{13}C,^{15}N-GNNQ]QNY (F2) and (b) diluted GNN[U-^{13}C,^{15}N-QQNY] (F4).

nances, with ^{13}C chemical shift differences up to 1.5 ppm. However, the other resonances also show significant differences between the forms, with the largest differences in the Asn-Cβ resonances (e.g., a 3.4 ppm difference between Asn_9-Cβ in fibrils 2 and 3). In these spectra we also observe a varying degree of difference with respect to the (monoclinic) crystalline peptide, with none of the fibrils matching the crystals exactly. The latter is clearly illustrated in panel d, which displays the same region for an isotopically dilute sample prepared at a peptide concentration of 12 mg/mL (F3). In this sample we observe the formation of monoclinic crystals (for which the resonances are connected by dashed lines) as well as the three fibril forms.

To facilitate a more detailed discussion, we have used the published monoclinic structure as a framework for examining the distribution and extent of the chemical shift variations within the peptide (Figure 12). The different extents of chemical shift deviation are color coded from black (no change) through green/yellow, to red (largest change), while nondetermined or missing resonances (e.g., for the flipping Tyr ring of the orthorhombic form or as yet unlabeled/unassigned positions) are colored gray.

From these figures one can arrive at the following interesting observations. Comparison of the orthorhombic and monoclinic crystals (Figure 12a) shows that the smallest chemical shift changes are clustered around the Gln_{10} residues and the directly surrounding nuclei (black/blue color). In the monoclinic crystals, the Gln_{10} side chains of the two monomers were found to be the core of the so-called "dry interface" within the unit cell. The lack of change in chemical shift might indicate that a similar interaction is maintained in the orthorhombic crystal form. The larger differences are in the positions facing the larger water clusters between the monomers and include a change in the dynamic behavior of the Tyr ring that now appears able to undergo a 2-fold flipping motion.

As discussed above, the smallest changes among the fibril forms, in comparison to the monoclinic crystals, are found for fibril 3, which is the least abundant fibril species. As can be seen in panel d, again the smallest changes are clustered around Gln_{10} with larger deviations toward the ends of the amino acid side chains. This could be indicative of this fibril having a similar core arrangement but a different packing scheme compared to the monoclinic crystals.

The two more dominant fibril forms display significantly larger deviations from the monoclinic crystals (or orthorhombic crystals). However, these two forms are also rather distinct from each other. As mentioned earlier, the intermediate intensity cross-peaks from fibril 2 actually indicate a number of resonances that are more consistent with a (local) α-helical structure rather than the expected β-sheet character typical of amyloid structures (refer to Figure 8). Panel c, showing this form, also indicates that the chemical shift deviations are distributed throughout the peptide, consistent with an overall change in the

Table 6. Overall Chemical Shift Deviations between the Different Aggregate Forms[a]

	monoclinic		orthorhombic		fibril 1		fibril 2		fibril 3	
	^{13}C	^{15}N	^{13}C	^{15}N	^{13}C	^{15}N	^{13}C	^{15}N	^{13}C	^{15}N
monoclinic			1.1	2.0	1.6	2.9	2.1	5.6	**1.1**	**1.5**
orthorhombic	**1.1**	**2.0**			1.4	2.9	2.0	6.1	1.1	2.2
fibril set 1	1.6	2.9	1.4	2.9			**1.0**	**1.9**	1.6	4.6
fibril set 2	2.1	5.6	2.0	6.1	**1.0**	**1.9**			1.8	4.8
fibril set 3	**1.1**	**1.5**	1.1	2.2	1.6	4.6	1.8	4.8		

[a] Deviations are shown as the rmsd (in ppm) between any two polymorphs, based on all ^{13}C or ^{15}N assignments common to both forms (but excluding the mobile Tyr positions). The most similar pair in each row is indicated in bold.

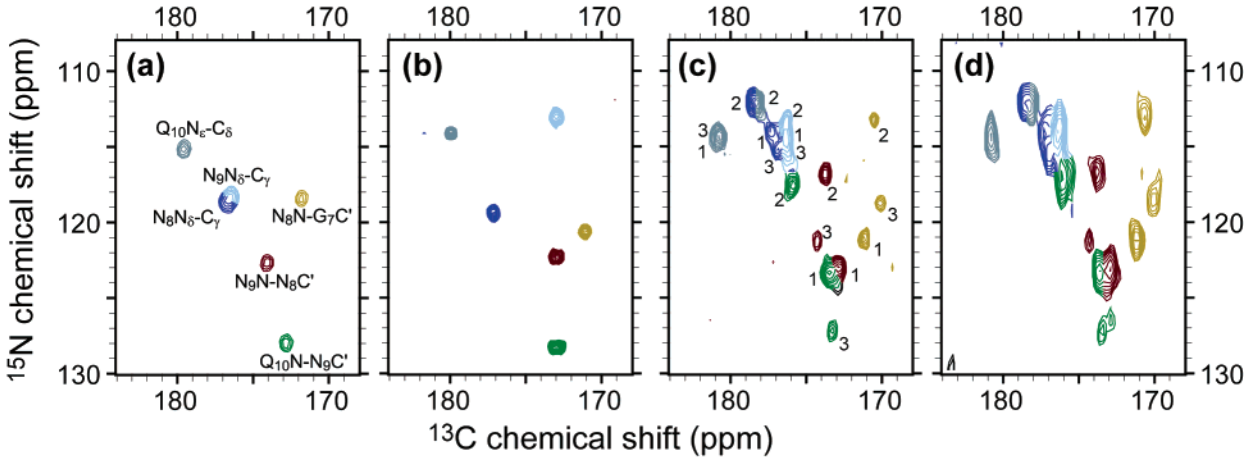

Figure 10. Comparison of the 2D $^{15}N-^{13}CO$ correlation spectra of [U-^{13}C,^{15}N-GNNQ]QNY for the two nanocrystalline forms: (a) monoclinic; (b) orthorhombic. Panels c and d show spectra obtained from the two independent fibril samples F1 and F2. The assignments of the color-coded peaks are indicated in panel a. Panel c includes the fibril form designations for the color-coded peaks. Data were acquired at (a) 500 MHz and (b−d) 700 MHz ^1H field, respectively.

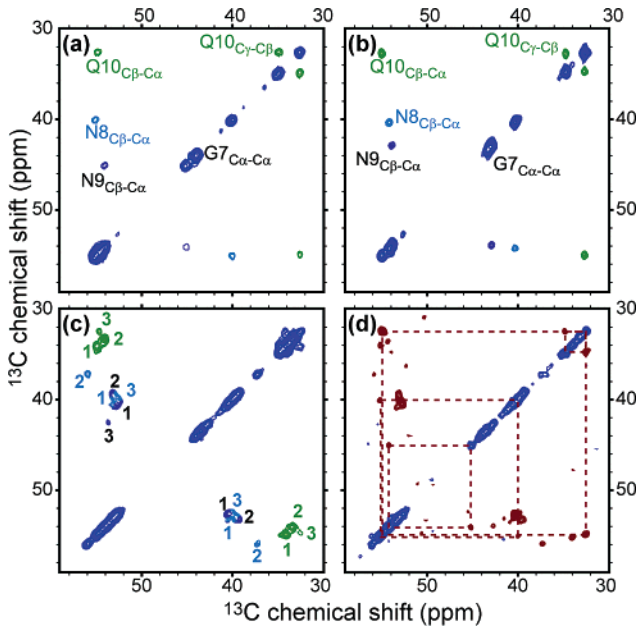

Figure 11. Comparison of the aliphatic $^{13}C-^{13}C$ correlations of (a, b) monoclinic and orthorhombic crystalline and (c, d) fibril forms of [U-^{13}C,^{15}N-GNNQ]QNY (samples F1, F3). Cross-peaks in panels a−c are color coded by residue, with the fibril forms marked by number in panel c. Panel d shows the coexistence of monoclinic crystals (dashed lines) and fibrils in a sample prepared at 12 mg/mL.

structural fold. The fibril 1 appears to more closely follow the predicted β-sheet character, but the significant chemical shift differences and their distribution make it unclear to what extent the structure resembles either of the crystalline forms. Still, it is interesting to point out that, analogous to the situation with fibril 3, the smallest differences are localized in the side chain of Gln_{10}.

Discussion

Polymorphism in GNNQQNY Aggregation. Using isotopically labeled and unlabeled peptides, we have generally reproduced the polymorphic aggregation behavior that previous publications[25−27] reported for the GNNQQNY peptide. At high peptide concentrations, >10 mg/mL, we observed formation of GNNQQNY fibrils that, on the basis of TEM data, resemble those previously reported.[27] As we reduce the concentration to around 10 mg/mL the formation of nanocrystals becomes favorable. Under our particular conditions, and in the absence of seeding, we consistently obtained monoclinic rather than orthorhombic crystals. Lowering the concentration further reduces the propensity for, and rate of, crystal formation, unless the sample was agitated (swirling). This appears to match the observations by Diaz-Avalos et al.,[27] who report a complete absence of aggregation below 5 mg/mL. Note that this is in contrast to experiments described by Eisenberg et al.[25,26] who observed the formation of fibrils under these conditions. Despite several attempts under a variety of conditions, we have as yet been unable to reproduce the formation of fibrils in the peptide concentration regime 1 mg/mL and below. We observed mostly a large decrease in the rate of the crystallization process that at times took many days rather than the few hours or less near 10 mg/mL. Agitation resulted in accelerated crystallization, something that was not previously reported. While the crystals resulting from this procedure might be of smaller size, making this approach less interesting for the preparation of X-ray

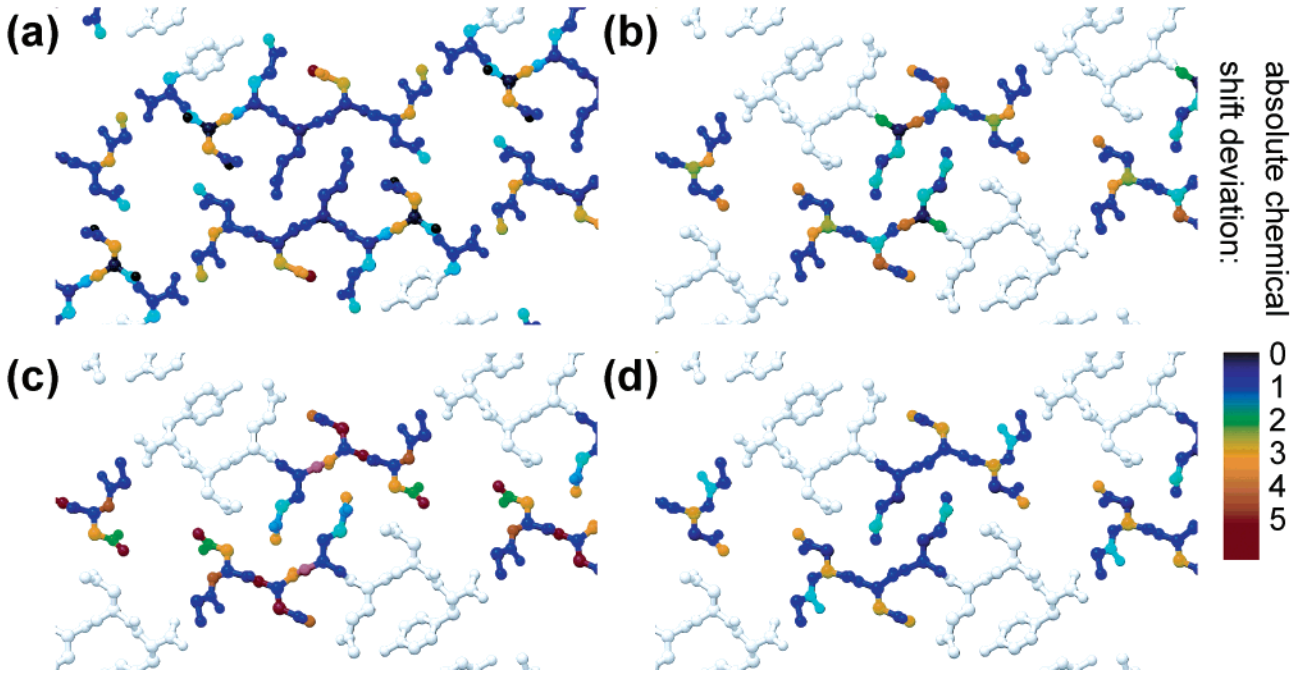

Figure 12. Illustration of chemical shift deviations between aggregate forms, projected onto the monoclinic crystal structure. We show the absolute chemical shift deviation (in ppm) relative to the monoclinic nanocrystals for the (a) orthorhombic crystals or (b−d) each of the three dominant fibril forms 1−3. The graphics were generated using UCSF Chimera.[93]

diffraction samples, they are more than suitable for SSNMR experiments because they maintain a high level of overall sample homogeneity. In our hands, the formation of orthorhombic crystals was less common than the monoclinic form and appeared most frequently under lower concentration conditions and with agitation of the sample container.

Our TEM results are consistent with descriptions of crystals and fibrils previously reported,[25−27] with the main difference being that we used crystals of substantially smaller size than the micrometer-sized crystals used in the X-ray experiments. TEM's of the fibrils show extended ribbonlike fibers that have lengthwise striations, at 5 nm distances. This closely resembles observations by Diaz-Avalos et al.,[27] who identify these as indications of protofilaments within the larger fibrils. We observe the presence of a variety of widths for these fibers, reflecting different multiples of the protofilaments (as indicated by the striations), but see no obvious indication of other polymorphism in the TEM results. Powder X-ray scattering data on the crystalline samples also matched the predicted or published reflections for the monoclinic and orthorhombic forms (data not shown).

In summary, the variety of GNNQQNY aggregates described here represent a number of forms that have been discussed in the existing literature. The salient feature of the solid-state NMR spectra is that we can resolve the spectra of the individual species and each of these forms—crystals and fibrils—under identical experimental conditions and compare them directly. Here, we report the observed resonances for the different atomic positions in the peptide, allowing us to perform an initial qualitative comparison. Both crystalline forms display narrow lines that suggest a high level of microscopic sample homogeneity and no indication of structural polymorphism *within* either crystal form. During the sample preparation procedures we do observe the coformation of different aggregate forms. This mostly involves the coexistence of monoclinic crystals and fibril material (see Figure 11d) rather than of both crystal polymorphs. However, in one predominantly orthorhombic sample, we did observe the initial coexistence of a small amount of monoclinic crystals (data not shown). Interestingly, the NMR spectra indicated that over time the monoclinic signal decreased and eventually disappeared after several days, suggesting a structural conversion between the two forms. Similar interconversion of crystal forms has been observed in X-ray diffraction experiments (D. Caspar, personal communication).

The NMR spectra of the fibrils clearly show the coexistence of three distinct, but self-consistent, sets of resonances with chemical shifts that are remarkably reproducible between different sample preparations. This holds true when the preparation method is varied, e.g., with changes in the peptide concentration between 12 and 25 mg/mL, with different fibrillization temperatures ranging from 4 to 30 °C, with variations of the pH during fibril formation, and with lyophilization and subsequent rehydration of the sample. Despite extensive attempts to modify the sample composition through variations in the fibrillization conditions, we have observed only small variations in the relative intensities of the NMR signals for each of the different fibril forms. The three forms are close to equal in intensity; therefore, the dominant form is so by only a small margin. Thus, normal intensity variations in the spectra can shift the identity of the dominant form from one fibril form to another. These observations raise the question as to the origin of the three signals observed from the fibrils. In particular, do the three NMR signals arise from three independent polymorphs present in the sample, or do the three signals represent multiple different conformations embedded in the same fibril? In the EM data we do not observe clearly distinguishable fibril morphology, but this may simple mean that the resolution of the micrographs is not sufficiently high to detect the conformational differences. However, if the three different conformers are present in the same fibril, then we might expect to observe polarization

exchange between the different forms via spin diffusion. For example, we have observed multiple intersheet contacts in ZF-TEDOR, R^2W, and spin diffusion spectra of fibrils from TTR105−115 and its L111M mutant (V. S. Bajaj, M. Caporini, A. Fitzpatrick, C. MacPhee, C. M. Dobson, and R. G. Griffin; to be published). However, in a number of $^{13}C-^{13}C$ DARR/RAD experiments on 100% isotopically labeled [U-^{13}C,^{15}N-GNNQ]QNY fibrils using long mixing times (up to 800 ms), we have not observed additional cross-peaks in the spectra. Because of the absence of these cross-peaks we do not have evidence that the three conformers are in intimate contact with one another. Thus, for the present we suggest that the signals arise from three different fibrils with different structures, but with morphological differences that are beyond the detection limits of the electron micrographs.

Spectroscopic Differences: Crystal Forms. The NMR data allowed us to precisely determine the ^{13}C and ^{15}N chemical shifts in both crystalline forms and for over half of the residues in the fibril forms. The assigned resonances combined with the more qualitative data presented for the latter half of the fibrils allow an initial comparison of structural features. While it is hard to establish precisely the origin of the differences, they are likely due to changes in the local conformation. Pending the completion of the full fibril assignments as well as more quantitative experiments, we will discuss the observed differences and similarities.

For this analysis, the obvious reference point is the published X-ray structure of the monoclinic crystalline form, with particular consideration for the various features that are proposed to be general for amyloid fibril formation. The "steric zipper" thought to form the core of the peptide−peptide interactions involves the even-numbered residues—N_8, Q_{10}, and N_{12}. When we compare the two crystalline forms, we note that the chemical shifts and torsion angles are not that different, especially compared to some of the fibril forms. The largest similarities are centered around Gln_{10}, which is at the center of the monoclinic crystal's "dry interface", while the largest difference is in the dynamic behavior of the Tyr_{13} aromatic side chain. The aromatic region of the monoclinic crystalline form shows the presence of distinct ϵ,ϵ' and δ,δ' ^{13}C's indicating that the Tyr side chain is completely immobile, whereas in the orthorhombic peptide these intensity of these resonances are attenuated, due to the 2-fold motion of the Tyr aromatic ring. This distinction would suggest that the steric Tyr−Tyr interactions that immobilize the ring in the monoclinic crystals (and constitute the main direct peptide−peptide interactions across the "wet interface" as illustrated in Figure 13) are absent in the orthorhombic crystals. Overall, the distribution of the similarities and differences throughout the peptide might be consistent with a structure that has a similar, close pairwise peptide−peptide interaction not unlike the monoclinic crystal but could have a different packing arrangement of such units within the unit cell. Note that previous X-ray analyses already indicate that the orthorhombic unit cell should contain four rather than two peptides, in contrast to the monoclinic unit cell.[27]

Spectroscopic Differences: Fibrils. Of more interest than the comparison of the two crystal forms is the structural study of the fibrils formed by the peptides. Previous studies have shown that fibrils formed by GNNQQNY display features similar to that seen for amyloid formation in general and the behavior of the Sup35p system in particular. In the MAS NMR spectra we have observed three distinct sets of resonances in all of the fibril preparations. In at least two of these fibrils (forms 1 and 3), we see that they conform to the general features expected for amyloid fibrils, in that their NMR chemical shifts are consistent with an entirely β-strand type structure. Beyond that, fibrils 1 and 3 also share some features with the crystal forms, the highest level of similarity being in the chemical shifts observed for Gln_{10} located at the core of the steric zipper in the monoclinic crystals. However, other regions of the peptide show significant deviations from the monoclinic resonances. Again, one notable difference between the monoclinic crystals and any of the other forms is correlated to the Tyr side chain.

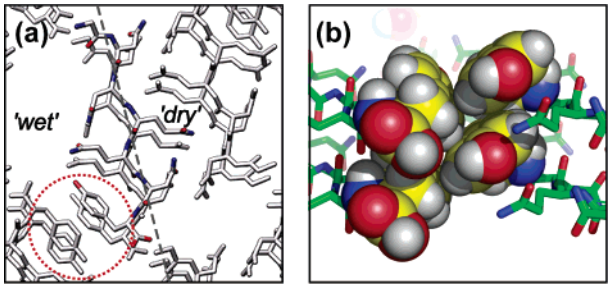

Figure 13. Illustration of the Tyr−Tyr contacts in the monoclinic crystals. Panel a contains a view along the fibril axis, highlighting the interactions of stacked Tyr across the "wet interface" between peptide monomers. The sideways view in panel b, with space-filling Tyr residues, illustrates the steric interactions limiting the ring dynamics in the monoclinic crystals. The graphics were generated using UCSF Chimera and Pymol.[93,94]

More unusual (and unexpected) for an amyloid-like fibril is that one of the conformers in the fibril samples (form 2) shows a significant number of chemical shifts that deviate from the values expected for β-strand secondary structure. As a result, this form also has the largest deviations from both crystalline forms. Due to the mixed nature of the samples, it is not clear which of the fibers seen in the TEM data correspond to a particular NMR spectrum. It is therefore unclear what the macroscopic nature of this particular "fibril form" is. The relatively narrow line widths of the associated resonances and highly reproducible preparation under a variety of conditions would suggest that it is unlikely to be an inhomogeneous and nonspecific aggregation of peptide. On the other hand, the observation of the signals via a CP mechanism indicates that they cannot correspond to a (residual) soluble fraction. An intriguing observation made by others is the indication of α-helical (non-β) structure in oligomers formed by the Sup35p protein during the process of fibril formation.[24]

Implications. In this section, we focus on the fibrillar forms that appear β-sheet in nature and examine the various aspects of the proposed core-fold and other features of the monoclinic crystal structure. The data we have are consistent with a certain level of similarity that is centered around the core residue of the steric zipper (Gln_{10}), which forms a self-complementary interaction across the dry interface of the monoclinic crystal assembly. Other residues show more significant deviations. One remarkable difference involves the Tyr side chain. As illustrated in Figure 13, the aromatic side chain forms an extensive close interaction in the monoclinic crystal structure, seemingly stabilizing it via aromatic $\pi-\pi$ interactions both within each β-sheet and between the sheets. And indeed, aromatic residues are thought to play an important role in the stabilization and

formation of amyloid-like structures including GNNQQNY aggregates.[34,92] In our NMR spectra, the extensive Tyr−Tyr interactions in the monoclinic crystals are reflected in its absence of spectral averaging, characteristic of a largely immobile ring. In contrast, this residue is found to be mobile in the orthorhombic crystals and in the fibrils. This could indicate a significant structural difference in the packing of the peptide within these structures, with potential implications for the energetics of stabilization. This should also have a drastic effect on the nature of the wet interface which could display a more significant role in construction of these other forms. In this context, we note that the unit cell of the orthorhombic crystals is twice as large as the cell of the monoclinic crystals and is thought to contain four peptide monomers rather than two.

Conclusion

^{13}C and ^{15}N MAS NMR spectra provide detailed information on a variety of solid materials and have permitted us to examine the range of aggregates that the GNNQQNY peptide adopts. The GNNQQNY nanocrystals provide very narrow line widths indicative of a high degree of microscopic order, an observation consistent with experiments on protein microcrystals. The fibrils themselves are yet another illustration of the fact that the line widths of amyloid fibrils can be relatively narrow indicating that the fibrils, like the crystals, are microscopically well ordered despite being macroscopically disordered. The GNNQQNY crystals and fibrils are therefore very suitable for these types of experiments. The crystal and fibril data do suggest some (localized) commonalities between the conformations of the various GNNQQNY species, in particular near the center of the "steric zipper". However, the data also show quite significant deviations from the monoclinic crystals, both in chemical shifts and in terms of mobility of the Tyr ring. These observations might support the idea that a steric zipper-like core is present in the fibrils, but variations elsewhere in the peptide remind us that significant questions remain concerning the assembly of such putative cores into actual fibrils. The presence of chemical shifts consistent with substantial non-β type structure in one of the fibril forms raises other intriguing questions.

One of the advantages of SSNMR is that it allows for numerous approaches to obtain detailed and quantitative structural information, in the form of distance and angular measurements. We are working on the application of such measurements to the GNNQQNY system to provide quantitative answers to the various questions raised by the current results. The preparation of more uniform fibril samples is part of the effort toward optimal application of these experiments. The study of the GNNQQNY peptide is instructive, not only in terms of the discussion of the basic structural features of amyloid fibers and their formation but also in providing a platform for the development and demonstration of techniques applicable for larger protein domains with similar characteristics.

Acknowledgment. We thank David Eisenberg, Ruben Diaz-Avalos, and Don Caspar for their suggestions and helpful discussions. Molecular graphics images were produced using the UCSF Chimera package from the Resource for Biocomputing, Visualization, and Informatics at the University of California, San Francisco, CA (supported by NIH Grant P41 RR-01081). This research was supported by the National Institutes of Health through Grants EB-003151 and EB-002026.

Supporting Information Available: A selection of 2D spectra used for assigning the orthorhombic GNNQQNY crystal resonances and spectra illustrating the assignment of each of the three forms in GNNQQNY fibril sample F1. This material is available free of charge via the Internet at http://pubs.acs.org.

JA068633M